Dynamics of Winds and Currents Coupled to Surface Waves

Peter P. Sullivan[1] and James C. McWilliams[2]

[1]Earth and Sun System Laboratory, Mesoscale and Microscale Meteorology Division, National Center for Atmospheric Research, Boulder, Colorado 80307-3000; email: pps@ucar.edu

[2]Department of Atmospheric and Oceanic Sciences and Institute of Geophysics and Planetary Physics, University of California, Los Angeles, California 90095-1565; email: jcm@atmos.ucla.edu

Annu. Rev. Fluid Mech. 2010. 42:19–42

First published online as a Review in Advance on August 4, 2009

The *Annual Review of Fluid Mechanics* is online at fluid.annualreviews.org

This article's doi: 10.1146/annurev-fluid-121108-145541

0066-4189/10/0115-0019$20.00

Key Words

boundary layer, Langmuir turbulence, wave breaking, large-eddy simulation, air-sea interaction, hurricane

Abstract

We discuss the coupling processes between surface gravity waves and adjacent winds and currents in turbulent boundary layers. These processes mediate exchanges of momentum, heat, and gases between the atmosphere and ocean and thus are of global significance for climate. Surface waves grow primarily by pressure-form stress from airflow over the waveforms, and they dissipate in the open sea by wave breaking that injects and stirs momentum, energy, and bubbles into the ocean. Wave motions pump wind eddies that control fluxes across the lower atmosphere. Flow separation occurs behind steep wave crests, and at high winds the crests flatten into spume, which diminishes the drag coefficient. In the ocean the Lagrangian-mean wave velocity, Stokes drift, induces a vortex force and material transport. These generate Langmuir circulations penetrating throughout the boundary layer and enhancing entrainment at the stratified interior interface in combination with other turbulent eddies and inertial-shear instability.

1. INTRODUCTION

ABL: atmospheric boundary layer

OBL: oceanic boundary layer

The marine atmospheric boundary layer (ABL) and oceanic boundary layer (OBL) are teeming with small- and large-scale flow processes. Spray, bubbles, turbulence, vortical structures, buoyant plumes, and surface and internal waves are important fluid dynamical processes that populate the boundary layers and influence the important vertical transport of momentum and scalars. The ABL and OBL connect fluxes at the boundary and interior interface similar to the terrestrial ABL and to engineering wall-bounded flows. They are distinctively characterized by high Reynolds number, stratification, and perhaps most importantly by coupling that is through a dynamic interface shaped by gravity waves. The surface waves that develop and connect the ABL and OBL span wavelengths ranging from millimeters to hundreds of meters, depending on the duration and magnitude of the wind forcing. The surface wave field moves randomly, propagates rapidly, supports wind stress, breaks intermittently, forces winds in the atmosphere, and induces Langmuir circulations (LCs) in the ocean. Surface gravity waves interact with turbulent winds and currents in surprising and beautiful ways, as demonstrated by the sea surface under high wind conditions (**Figure 1**).

The vertical dimensions of the ABL $\mathcal{O}$ (500 m), OBL $\mathcal{O}$ (50 m), and surface wave field $\mathcal{O}$ (5 m) are quite modest compared to the overall height and depth of the atmosphere and ocean. Nevertheless, boundary-layer turbulence and surface waves play a critical role at larger scales as they regulate the functioning of Earth's climate and weather systems. Coupling of the atmosphere to the ocean through wave processes is particularly important and impacts numerous scientific and engineering air-sea disciplines. Climate forecasts are dependent on the turbulent exchange of momentum and scalars at the air-sea interface and at the depth of the ocean mixed layer (Large et al. 1994, McWilliams 1996). Wave breaking and the subsequent generation of bubbles and spray control gas exchange (D'Asaro & McNeil 2007, Wanninkhof et al. 2009), impact stratocumulus-cloud-deck formation (Stevens et al. 2003), alter ocean acoustics (Melville 1996), and influence the remote sensing of sun glitter (Munk 2009). Hurricane intensity and track predictions are crucially dependent on the air-sea-interface drag and enthalpy coefficients and the

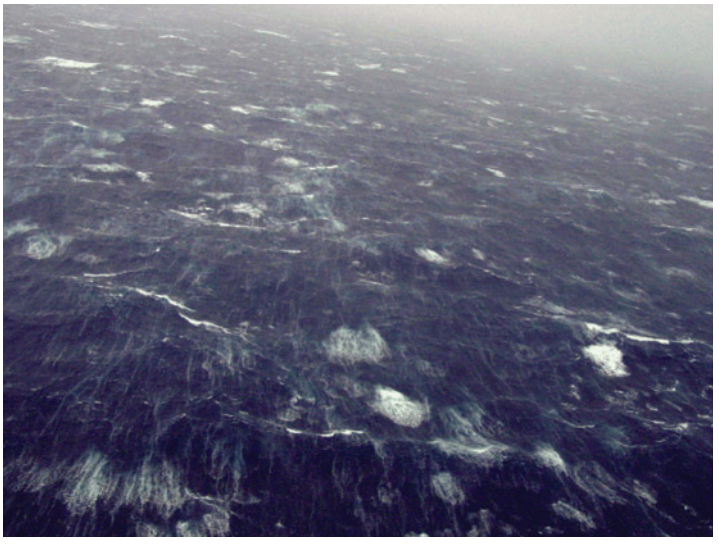

Figure 1

Photograph of sea-surface and breaking waves in Hurricane Isabel taken from a low-level flight during the CBLAST field campaign (Black et al. 2007). Image provided by Michael Black.

mixing efficiency of the OBL (Emanuel 2004, Sanford et al. 2007). Turbulent hurricane wakes also generate plankton blooms through the entrainment of cool fresh water at the base of the thermocline (Lin et al. 2003). Statistical wave-prediction models rely heavily on parameterization of the wind-input (wave growth) and dissipation (wave breaking) terms that appear as source terms in the wave-action equation (Komen et al. 1994, Janssen 2008).

CBLAST: coupled boundary-layers air-sea transfer

TKE: turbulent kinetic energy

The present understanding of the fundamental processes that connect winds, waves, and currents is partly inhibited by the challenging task of acquiring outdoor observations: Platform movement, sensor technology, cost, and broadband variability of the atmosphere, ocean, and wave fields all limit the acquisition of observational data sets in the marine surface layers. The CBLAST (coupled boundary-layers air-sea transfer) field campaigns (Black et al. 2007, Chen et al. 2007, Edson et al. 2007) are recent attempts to connect marine boundary layers over a range of wind speeds, taking into account the importance of waves in the coupling process. Data interpretation in an air-sea environment is difficult: Moving platforms alter the measurement of vertical momentum and scalar fluxes (Graber et al. 2000), and the large nearly irrotational motions associated with waves swamp the signal from turbulent currents, making the creation of even turbulent kinetic energy (TKE) budgets in the upper ocean challenging compared with its atmospheric counterpart.

Computational simulation of the marine boundary layers is equally challenging. Computer power (Bement 2007) is not capable of resolving all scales in a high–Reynolds number turbulent surface layer (Pope 2000, p. 346). Furthermore, existing numerical algorithms cannot capture a mobile wave field that breaks intermittently and spans scales ranging from small-scale bubbles, $\mathcal{O}$(1 mm), to long-wavelength swell, $\mathcal{O}$(150 m). One-dimensional (1D) column models of the marine boundary layers relegate wave effects into an effective surface roughness by analogy with the terrestrial ABL (Donelan 1998). Direct coupling of air and water under steady-state conditions that account for different physical properties (density, viscosity) is possible using turbulence closures (Eifler 2005) but is only applicable to low-wind situations in which waves have small amplitude and do not break. Wave processes and their coupling to the marine boundary layers are poorly represented or neglected in weather and climate models.

The topic of air-sea coupling is extensive, and the current review can only address a few elements of the coupling process. Free-surface flows are intriguing (Tsai & Yue 1996), and the computational algorithms used to study these flows are evolving to include a wider spectral range of scales, but they are intentionally omitted from this limited review. Broader descriptions of air-sea interaction phenomena can be found in Csanady (2001), Melville (1996), Phillips (1977), and Thorpe (2005).

Our perspective of atmosphere-ocean interaction described here focuses on small-scale processes and adopts a two-step conceptual view of the coupling between air and water. In this model, the primary job of surface winds is to supply momentum and energy to grow and maintain the wave field, as outlined in Section 2. Waves drive currents and energize the ocean boundary layer through wave-current interactions and wave breaking as discussed in Section 3. The marine boundary-layer culture has roots firmly cemented in Monin-Obukhov similarity theory (also known as the law of the wall) near the wave interface outside of a thin-diffusive sublayer. One of our themes is to examine under what conditions this is true.

2. WINDS AND WAVES

Here we introduce terminology and nomenclature that commonly appear in our discussion. Variables with subscripts $()_{a,o}$ denote atmospheric and oceanic quantities, respectively. Hence the air and water fluid densities are (ρ_a, ρ_o). As is common in all geophysical boundary layers, the near-surface turbulent stresses in the ABL and OBL are $\boldsymbol{\tau}_{a,o}$, and by analogy with solid-wall boundary layers, they define friction velocities $u_*|_{a,o}$; i.e., $u_* = \sqrt{|\boldsymbol{\tau}|/\rho}$.

We refer to the basic properties of a surface gravity wave: A propagating monochromatic surface wave has height $\eta = a\ \cos[k(x - ct)]$, where a is the amplitude and (k, λ) are the wave number and wavelength linked to the phase speed c by a (deep-water) dispersion relation $c^2 = g/k = g\lambda/2\pi$ with g gravity. The wave has radial frequency $\omega = kc$, slope (or steepness) $= ak$, and energy $E = \rho_w g a^2/2$ (e.g., Lighthill 1978).

In the wind-wave-current literature, the ratio c_p/u_{*a}, where c_p is the phase speed of the peak energy in the wave-height spectrum, is called the wave age. Under idealized conditions (in local equilibrium with the wind), the properties of wind waves depend only on fetch (or distance from shore), friction u_{*a}, and gravity g. Wave age serves as a surrogate variable for fetch (Csanady 2001, p. 11). Often the literature also refers to wave age as c_p/U_a, where U_a is a reference surface wind speed usually measured at the height $z = 10$ m in outdoor observations. When Monin-Obukhov similarity theory holds, there is a direct conversion between wind speed and friction velocity. We use both c_p/u_{*a} and c_p/U_a in our discussion. When winds and waves reach equilibrium or full development (i.e., wave field statistics are stationary), $c_p/u_{*a} \sim 30$ and $c_p/U_a \sim 1.2$ (Alves et al. 2003). Growing seas are $c_p/u_{*a} < 30$ or $c_p/U_a < 1.2$, which we call the wind-driven wave regime. Old seas are $c_p/u_{*a} > 30$ or $c_p/U_a > 1.2$, which we call the wave-driven wind regime.

2.1. Wind-Driven Waves

Under the action of wind, wave amplitude and energy generally vary exponentially with time (e.g., Miles 1957),

$$a(t) = a_o e^{\omega\zeta t/2}, \quad E(t) = E_o e^{\omega\zeta t}, \tag{1}$$

with the fractional input of energy to the wave

$$\zeta = \frac{\rho_a}{\rho_w}\beta, \tag{2}$$

where β is a dimensionless growth rate. β can be written in terms of surface pressure and viscous stresses (e.g., Belcher & Hunt 1998, Mastenbroek et al. 1996) but is dominated by the correlation between surface pressure and wave slope $\langle p\eta_x \rangle$, i.e., by the surface-form stress or drag (Donelan 1999, Donelan et al. 2006). Determining the dependence of sea-surface drag on environmental conditions (e.g., wind speed, wave age, wave height, wave slope, and wind-wave alignment) still remains a core focus of wind-wave research (Jones & Toba 2001).

Direct field measurements of the wave-induced pressure in airflow over waves are rare, and consequently there is a dispute about the underlying mechanisms leading to wave growth. Belcher & Hunt (1998) provide an extensive review of their theory for flow over water waves based on the asymptotic scalings used in turbulent flow over low hills. The theory exposes the delicate coupling between surface pressure distribution and the overlying turbulence. Far from the surface, the turbulence evolution is assumed to be dominated by mean flow straining in which rapid distortion theory applies. Close to the surface, the turbulence timescale is fast compared to mean advection over the wave; turbulence is then in local equilibrium with production, balancing dissipation. Spatially varying pressure gradients working on turbulent stresses in the inner region lead to asymmetrical streamline thinning and thickening around a wave crest, which leads to a net form drag without flow separation, i.e., nonseparated sheltering. (The pressure drag induced by turbulent boundary-layer growth over an airplane wing is a broadly similar mechanism.) The experimental data of Mastenbroek et al. (1996) provide some support for the rapid distortion mechanism in the outer region.

The competing physical interpretation for the growth of wind waves is the critical-layer mechanism first pioneered by Miles (1957) and refined by several authors (Janssen 1991); it still remains a basis for parameterizing wave growth in statistical wave models (Janssen 2008). In a frame of reference moving with the phase speed of the wave, a critical level (layer) develops at the height at which the wind speed $u = c$, roughly $z_c \sim z_o e^{\kappa c/u_{*a}}$ (where z_o is the roughness of the surface and κ is the von Kármán constant). Lighthill (1962) interpreted the Miles mechanism in terms of vorticity redistribution at the wave surface, and Janssen and colleagues (Komen et al. 1994, chapter II) showed how the Miles instability relies on negative curvature in the wind profile. The Miles mechanism is difficult to test with measurements because a logarithmic wind profile with curvature $\partial^2 u/\partial z^2 \sim -1/z^2$ has an absolute maximum near the edge of the viscous sublayer (Phillips 1977, p. 128). Hristov et al. (2003), using novel signal processing (Hristov et al. 1998), obtained convincing observational evidence for critical layers associated with long waves (i.e., well above the surface where the mean flow gradients are relatively weak). A difficulty in assessing the importance of nonseparated sheltering dynamics versus critical-layer dynamics is that both occur simultaneously for wind-driven waves.

Despite continued refinement, the existing theories and models are unable to reconcile their predictions of wave growth with available measurements, thus hinting at missing dynamics. Model predictions are systematically low by roughly a factor of two compared to measurements by Peirson & Garcia (2008, their figure 4) and Belcher & Hunt (1998, their figure 8). Peirson & Garcia (2008) re-examined existing data sets, as well as provided new measurements, and concluded that wave slope is a critical missing ingredient. Their analysis shows normalized β increases with decreasing ak. They proposed that a significant wave coherent tangential stress develops as a result of interactions between short waves riding on long monochromatic waves when $ak < 0.1$, whereas for $ak > 0.1$, the large surface drift associated with fast-moving waves effectively suppresses small waves by inducing rapid breaking.

A complementary approach to theory and measurements is to examine turbulent flow over moving waves using turbulence-resolving direct numerical and large-eddy simulations (DNS and LES). In the case of DNS all scales—energy-containing eddies down to the viscous dissipation range—are resolved, but the limitation is low Reynolds number (Moin & Mahesh 1998). Geophysical LES with no explicit Reynolds number and with a z_o representation of surface roughness can be used to model the energy-containing range of outdoor flows, but with the uncertainty associated with modeling unresolved subgrid-scale motions (Hatlee & Wyngaard 2007, McWilliams et al. 1997, Moeng 1984, Sullivan et al. 2003).

There are only a handful of DNS solutions for turbulent flow over a propagating wave (Kihara et al. 2007, Shen et al. 2003, Sullivan & McWilliams 2002, Sullivan et al. 2000). Our solutions replicate features of laboratory experiments and outdoor observations. For a wave slope of $ak = 0.1$, the results show that surface waves influence the mean wind profiles, vertical momentum fluxes, variances, and surface pressure for wave ages $c/u_{*a} = [0{-}22]$. The form stress across c/u_{*a} is similar to predictions by second-order closure models but with a higher maximum at a lower wave age. Meirink & Makin (2001) attributed this to Reynolds number effects, and thus viscosity is a potential contributing factor to the underprediction of wave growth. Flow visualization of the horizontal velocity fields illustrates wind-wave coupling. The low-speed streaks characteristic of flat-wall boundary layers are disrupted by the imposed waves over a depth $z \sim 1/k$. Conditional sampling of the DNS flow fields identifies a region of closed streamlines (or cat's-eye pattern) centered about the critical-layer height, which adapt to the wave depending on c/u_{*a}. The maximum distortion of the time-averaged streamlines and the maximum drag occur when the critical layer is near the edge of the viscous sublayer, as suggested by Phillips (1977). These results show that critical layers persist and play a dynamical role in these low–Reynolds number DNS.

DNS: direct numerical simulation

LES: large-eddy simulation

2.2. Wave-Driven Winds

Over the open ocean, winds with significant space-time variability generate surface wave fields with broadband frequency. Hanley (2008) constructed climatological maps of wave age c_p/U_a from surface winds and wave-height spectra that show a rich mixture of growing and old sea states over the globe. The results are seasonally dependent, but generally in the storm tracks, strong winds force wave fields toward equilibrium, $c_p/U_a \to 1.2$, whereas in expansive tropical regions, light winds riding above swell lead to old sea states with $c_p/U_a > 1.2$. Swell waves are the long-wavelength components left over from previous and often remote wind-generation events. Swell can propagate long distances with little dissipation, move in arbitrary directions with respect to the local winds, and dominate the local wave field when winds are light, $U_a \sim \mathcal{O}(5\ \mathrm{m\ s^{-1}})$. Our surface-layer observations (Sullivan et al. 2008) find that swell frequently coexists and dominates local wind waves. The presence of swell makes the wave-driven wind regime $c_p/U_a > 1.2$ unique.

Swell can induce significant misalignment between surface winds and turbulent stress and generally invalidates the use of Monin-Obukhov similarity theory that assumes wind-stress alignment. Surface observations by Grachev et al. (2003) show the stress vector may deviate widely from the mean wind flow, including cases in which stress is directed across and even opposite to the wind when $U_a < 5\ \mathrm{m\ s^{-1}}$ or less. Also, in certain circumstances, wind following fast-moving swell induces momentum transport from the ocean to the atmosphere (Grachev & Fairall 2001, Smedman et al. 1999, Sullivan et al. 2008), i.e., in the opposite direction to the wind-driven wave regime (Section 2.1). This is accompanied by the formation of low-level jets, i.e., slightly super geostrophic winds in the region $z \sim 20$ m above the ocean surface (Donelan & Dobson 2001, Miller 1999). Meteorological conditions in the Baltic Sea frequently lead to a wind-following-swell regime in the aftermath of strong gales, and the above features were observed by Smedman et al. (1994, 1999). Surprisingly, Smedman et al. (1994) also found that the upper levels of the ABL are modified; e.g., they found vertical momentum flux $\langle u'w' \rangle > 0$ up to $z \sim 200$ m, which is opposite in sign to conventional shear-driven boundary layers above rough surfaces.

To examine interactions between atmospheric turbulence and swell, we adapted our LES model of the full marine ABL to include propagating sinusoidal modes at its lower boundary (Sullivan et al. 2008). The wave-driven wind regime is an ideal, but computationally expensive, LES problem. Long-wavelength swell modes with $\lambda \approx 100$ m are well resolved in a typical mesh (e.g., $1200 \times 1200 \times 800$ m with $250 \times 250 \times 96$ grid points), but the fast propagation speed $c_p \approx 12.5\ \mathrm{m\ s^{-1}}$ severely limits the computational time step, and the iterative solution for the pressure needed to satisfy $\nabla \cdot \mathbf{u} = 0$ is expensive. The process studies conducted include cases with stationary bumps, swell propagating with the wind, and swell propagating against the wind, all with the same large-scale but weak geostrophic pressure gradients. The wave age is $c_p/U_a > 2$, and reaching a statistically steady state requires more than 200,000 time steps.

The LES results corroborate and explain many of the curious observations in the wave-driven wind regime. The surface-layer winds are strongly coupled to the structure of the near-surface pressure field (i.e., the resolved surface-form stress). In flow over wind-opposing waves, the resolved-form stress acts as a drag on the winds, whereas for wind-following waves, it acts as a thrust. In the latter situation, LES predicts momentum transfer from the ocean to the atmosphere and the generation of a low-level jet; the magnitude of the winds at $z \sim$ [10–20] m is approximately 10% greater than the geostrophic wind and varies with surface heating. The jet formation results from a wave-induced turbulent momentum flux divergence that accelerates the flow and from a retarding pressure gradient, both of which are opposite to the momentum balance in classical shear boundary layers. In a neutrally stratified ABL, the presence of a low-level jet reduces the mean shear between the surface layer and the top of the ABL, leading to a near collapse of turbulence in the ABL.

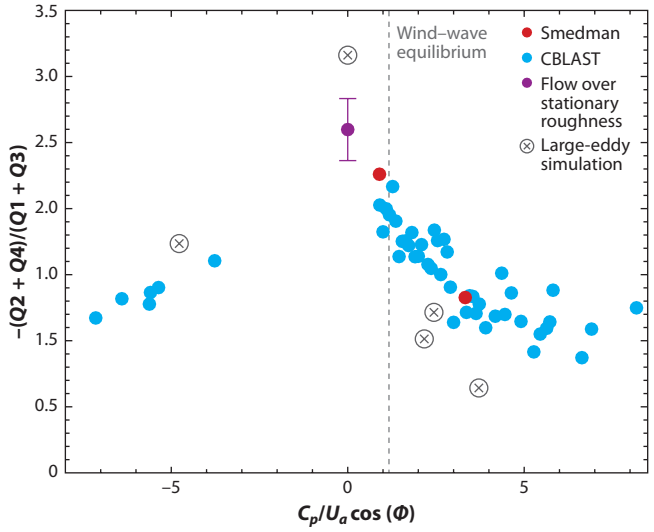

Figure 2

Quadrant analysis of the vertical momentum flux in the marine surface layer for varying wave age with wind-following and -opposing waves. Here wave age is corrected for the alignment angle ϕ between the wind direction and the wave-propagation direction. The quadrants are defined as $Q1^{(+)} = (u' > 0, w' > 0)$, $Q2^{(-)} = (u' < 0, w' > 0)$, $Q3^{(+)} = (u' < 0, w' < 0)$, and $Q4^{(-)} = (u' > 0, w' < 0)$. CBLAST results (Edson et al. 2007) are indicated by the blue circles; the observations of Smedman et al. (1999) are denoted by the red circles; results for flow over stationary roughness (note wave age $= 0$) are indicated by the purple circles; and large-eddy simulation results at $z \approx 15$ m above the surface are indicated by ⊗. For $c_p/U_a \cos\phi = 1.2$ and greater, waves transfer positive momentum to the atmosphere in quadrants $Q1$ and $Q3$, thus making the ratio $-(Q2 + Q4)/(Q1 + Q3)$ smaller. Figure taken from Sullivan et al. 2008 and used by permission from the American Meteorological Society.

The boundary-layer mean wind profile, turbulence variances, and vertical momentum flux are then highly dependent on the nature of the wave field. The LES predictions for the dependence of vertical momentum flux on wave age (**Figure 2**) are also found in field observations. Using a 1D column model of the neutrally stratified Ekman boundary layer, Hanley & Belcher (2008) and Makin (2008) demonstrated that low-level jets can be generated from a realistic full-wave spectrum and a simple model for the wave-induced momentum flux at the surface.

2.3. Steep Waves

Photographs of the wind-driven sea surface show a continually evolving pattern of small-scale waves with wavelength $\mathcal{O}$ (m) or less. These small-scale waves, termed microbreakers, grow rapidly; are steep, $ak > 0.1$; and frequently break without visible air entrainment (Banner & Peirson 1998). In general, steep and breaking waves introduce a new route to wind-wave coupling (e.g., flow separation) that is not considered in Sections 2.1 and 2.2. Donelan et al. (2006) and others advocate flow separation as an important missing mechanism in theoretical models of wave growth. Compared to the extensive literature on boundary-layer separation from solid surfaces, there are relatively few laboratory studies focused on separation over moving-water waves and almost none over the ocean (Donelan et al. 2006).

Laboratory experiments utilizing improved instrumentation are advancing the present understanding of this aspect of wind-wave coupling. Using visualization and particle image velocimetry,

Veron et al. (2007) and Reul et al. (2007) provide compelling and quantitative evidence for flow separation over young strongly forced wind waves. **Figure 3** shows instantaneous velocity vectors in a 2D vertical plane collected over a wind-driven water surface; the measurements extend down to the water surface and adequately sample the air viscous sublayer $z^+ \leq 10$. The disrupted streamline patterns downwind of the wave crest and the instantaneous spanwise vorticity contours are strong indicators of flow separation. In this image, there is scant evidence of wave breaking, which is the usual criterion used to predict the onset of separation (Banner & Melville 1976, Gent & Taylor 1977). Theoretical analysis assumes steep but symmetrical waveforms, whereas Reul et al. (2007) showed that waveform asymmetry is an important characteristic of separated flow over waves.

A separated flow region downstream of a wave crest strongly couples the near-surface viscous layer with the outer flow similar to flow past a backward facing step with the surface pressure field dependent on the location of the fluctuating reattachment point. Understanding the frequency and spatial extent of flow separation is important because pressure measurements at a fixed height over the ocean are often extrapolated to the surface, assuming potential flow (Snyder et al. 1981). This can be a source of error in estimates of the pressure wave-slope correlation and hence can lead to errors in the surface-drag calculation.

2.4. Drag Laws and High Winds

In outdoor flows, sea-surface drag depends on the form-stress distribution at scales ranging from capillaries to those beyond the peak in the wave spectrum. Predicting β in the presence of swell, breaking waves, and intermittent airflow separation across this scale range with LES or DNS is well beyond present computational ability. Large-scale weather and ocean-wave forecast codes, as well as climate-prediction models, rely on the bulk aerodynamic drag formula

$$\boldsymbol{\tau}_a = \rho_a C_d |\mathbf{U}_a| \mathbf{U}_a, \tag{3}$$

which determines the atmospheric momentum flux $\boldsymbol{\tau}_a$ in terms of the wind vector $\mathbf{U}_a$ and a drag coefficient C_d. All the wind-wave coupling processes are lumped into a single unknown transfer coefficient. Observational studies utilize eddy correlation or inertial dissipation measurements of turbulent flux to determine C_d (Edson et al. 2007). The use of Equation 3 is based on the assumption that $\boldsymbol{\tau}_a$ obeys Monin-Obukhov scaling in the surface layer (Fairall et al. 2003).

A large body of observational evidence confirms that C_d varies linearly with wind speed over the range [5–25] m s^{-1} with slight variations due to sea state. In the lower wind-speed range, $U_a < 5$ m s^{-1}, Edson et al. (2007) showed wide scatter in C_d measurements, partly because of sampling errors but also because of wave-driven winds caused by swell (Section 2.2). Wind-wave tank measurements (Donelan et al. 2004), shown in **Figure 4**, convincingly replicate the linear variation observed outdoors but also exhibit an unexpected trend—saturation for wind speeds above 30 m s^{-1}. Recent results collected in hurricanes verify the laboratory trends but find lower saturated values with a possible decrease at large U_a (Powell et al. 2003). Candidate mechanisms that are invoked to explain drag-coefficient saturation include spray generation (Bye & Jenkins 2006) and flattening of wave crests accompanied by extensive flow separation, which eliminates small-scale roughness in the wave troughs (Donelan et al. 2004).

A drag plateau impacts high-wind atmospheric and oceanic forecasts. As maximum hurricane intensity varies inversely with C_d (Emanuel 2004), a saturated drag coefficient leads to a prediction of more powerful storms. Ocean models are only able to match observations by utilizing a saturated C_d (Sanford et al. 2007, Zedler 2007); linear extrapolation of Large & Pond's (1981) drag coefficient to high winds significantly overestimates mixing in ocean models.

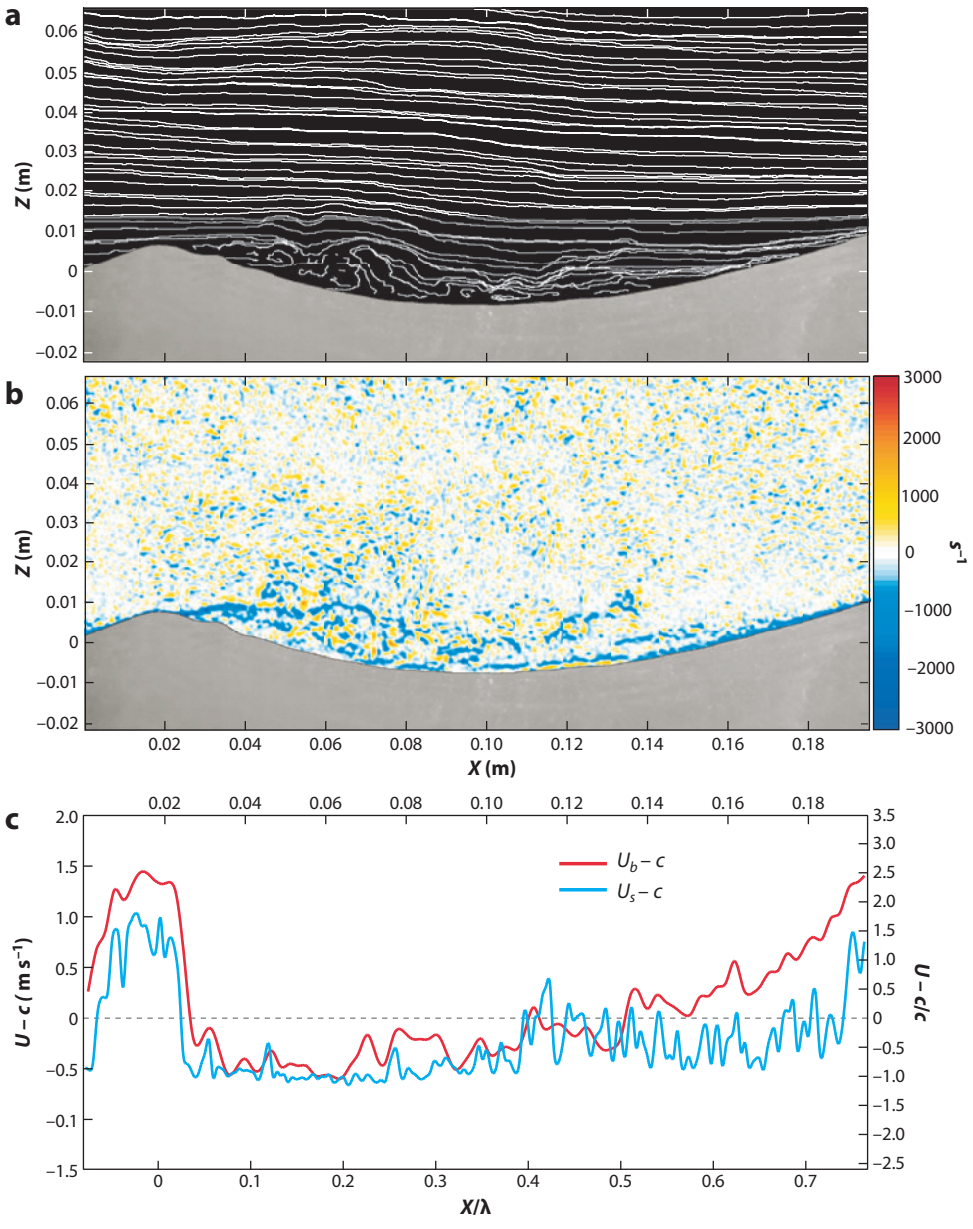

Figure 3

Separated airflow over a strongly forced laboratory wave from Veron et al. (2007). (*a*) The instantaneous streamline pattern for a wind speed $U_a = 5.7$ m s^{-1}; (*b*) the corresponding vorticity field; and (*c*) the near-surface estimates of the surface parallel velocity U_s and the average buffer-layer velocity U_b. The velocities are shown in a frame of reference moving with the phase speed of the surface wave c. (U_s, U_b) $- c <$ 0 in the separated flow region. Image provided by Fabrice Veron, used with permission from the American Geophysical Union.

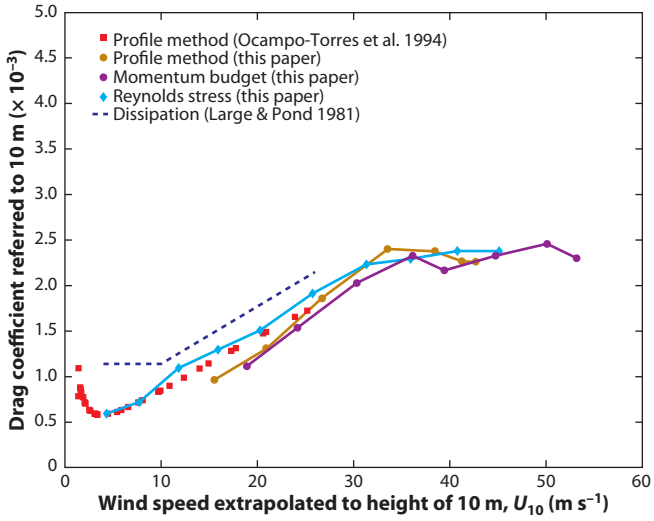

Figure 4

Variation of the neutral stability drag coefficient C_d with wind speed U_a derived from laboratory measurements using various methods from Donelan et al. (2004). The dotted line is the drag coefficient formula developed to fit the field measurements of Large & Pond (1981). Note the saturation at high wind speeds $U_a > 30$ m s^{-1}. Results provided by Mark Donelan, used by permission from the American Geophysical Union.

3. WAVES AND CURRENTS

3.1. Modeling Wave-Current Interactions with Vortex Forces

The widespread existence of LCs in outdoor flows (lakes, tidal channels, open ocean) over a wide range of forcing conditions has motivated the development of theoretical and numerical models of wave-current interactions (Leibovich 1983, Thorpe 2004). Conceptually, LCs are viewed as a steady array of counter-rotating vortices with their elongated primary axis aligned with the wind. A visual signature of LCs is the collection of surface foam and debris into meandering lines that often join in the downwind direction, as shown in **Figure 5*a***. Subsurface observations can track the evolution of LCs by following bubbles trapped in the downwelling regions between vortices using sidescan sonar (Smith 1998, Thorpe et al. 2003a), and LCs are identified in measurements collected from current profilers (Gargett & Wells 2004). LCs are regarded as an important coherent structure of (wavy) upper-ocean dynamics that coexist with shear eddies and buoyant plumes. This mixed regime of surface waves and unsteady currents is referred to as Langmuir turbulence (McWilliams et al. 1997).

The most compelling theoretical interpretation for the formation and evolution of LCs is as a wave-current instability first theoretically discovered by Craik & Leibovich (1976) with refinements discussed by Leibovich (1983). The fundamental Craik-Leibovich instability mechanism (CL2) relies on amplification of background current perturbations with vorticity $\boldsymbol{\omega}$ by a vortex force $\mathbf{u}^{St} \times \boldsymbol{\omega}$, where $\mathbf{u}^{St}$ is the Lagrangian mean-wave velocity or Stokes drift (see Leibovich 1983, figure 3). McWilliams & Restrepo (1999) and McWilliams et al. (2004) generalized and extended the CL theory to include wave effects in finite-depth water, and Lane et al. (2007) showed how wave-averaged equations follow from either a radiation-stress or vortex-force representation of the advection term $\mathbf{u} \cdot \nabla \mathbf{u}$. They found that vortex force is the dominant wave-averaged effect on currents outside the near-shore surf zone.

LC: Langmuir circulation

CL: Craik-Leibovich

CL2: Craik-Leibovich second form of instability

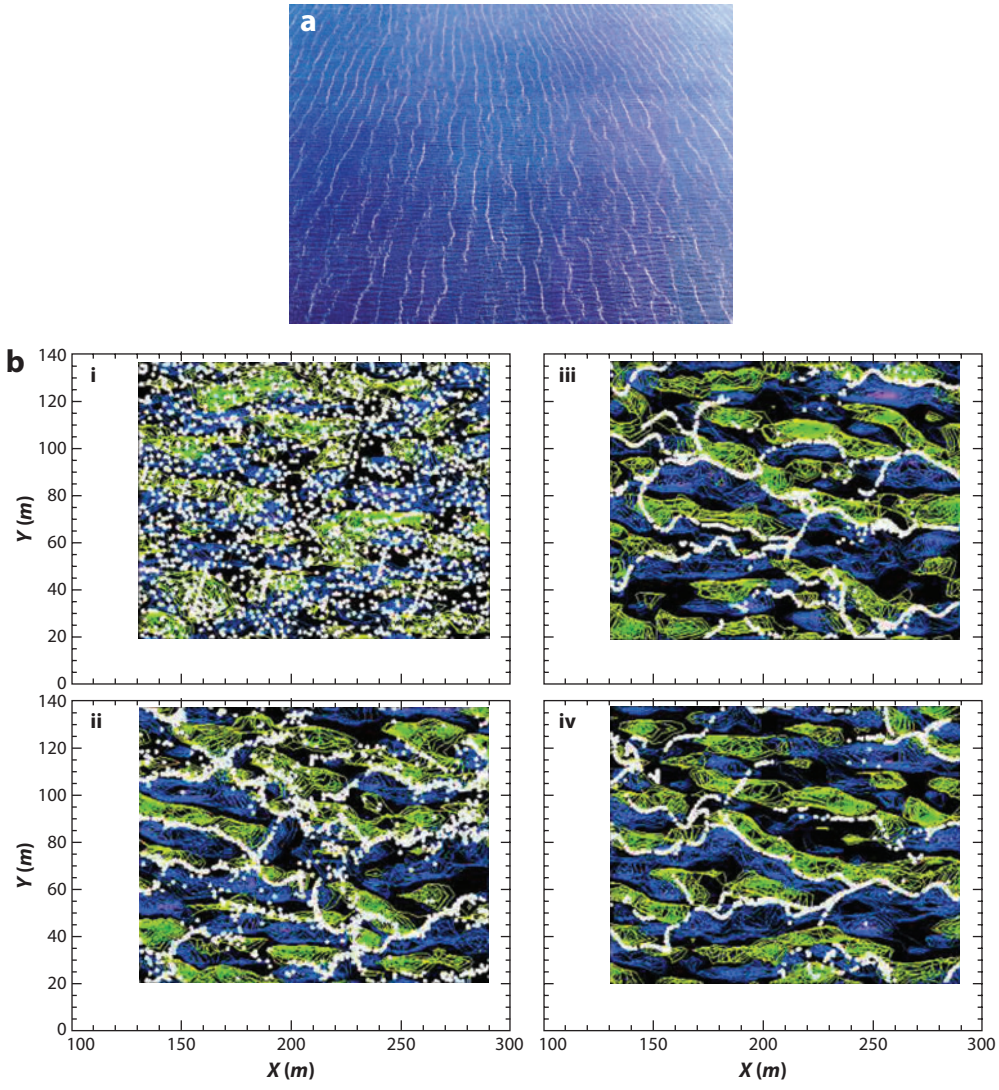

Figure 5

(*a*) Photograph of converging foam lines generated by Langmuir circulations in the Great Salt Lake (image provided by Stephen Monismith). (*b*) Movement of surface particles in large-eddy simulations from McWilliams et al. (1997). Particles are randomly released at $t = 0$ in panel *i*. Panels *ii*, *iii*, and *iv* show particle positions 480, 960, 1280 s later, respectively. The green and blue contours are positive and negative values of streamwise vorticity ± 0.0055 s^{-1} in the region $0 < z < 10$ m below the water surface. Notice the particle migration into the regions between the Langmuir cells and the mergers that occur at forward-looking Y junctions.

LES models with varying levels of wave effects (Grant & Belcher 2009, Harcourt & D'Asaro 2007, Li et al. 2005, Skyllingstad & Denbo 1995) are adding insight into turbulent OBL dynamics and, with increasing computer power, are able to simulate turbulent flows forced by a long-time wind history (Section 3.3). An example of an LES model, based on the CL equations, with wave effects is described by McWilliams et al. (1997) and Sullivan et al. (2007). The model is based on an incompressible Boussinesq formulation with a TKE subgrid-scale parameterization (Moeng 1984). Schematically, the governing CL equations for momentum, density, and subgrid-scale TKE

with wave-current interactions are

$$\frac{\partial \bar{\mathbf{u}}}{\partial t} = \ldots - f\hat{\mathbf{k}} \times \mathbf{u}^{St} + \mathbf{u}^{St} \times \bar{\boldsymbol{\omega}}, \tag{4a}$$

$$\frac{\partial \bar{\rho}}{\partial t} = \ldots - \mathbf{u}^{St} \cdot \nabla \bar{\rho}, \tag{4b}$$

$$\frac{\partial e}{\partial t} = \ldots - \mathbf{u}^{St} \cdot \nabla e - \tau_{i3} \frac{\partial u_i^{St}}{\partial x_3}. \tag{4c}$$

In Equation 4, $(\bar{\mathbf{u}}, \bar{\boldsymbol{\omega}})$ are resolved-scale velocity and vorticity, respectively; f is the Coriolis parameter; $\bar{\rho}$ is the density; e is the subgrid-scale TKE; and τ_{ij} is the deviatoric subgrid-scale stress tensor. The added wave effects are Coriolis-Stokes and vortex-force terms in Equation 4a, Lagrangian mean advection of material tracers in Equations 4b and 4c, and Stokes production of subgrid-scale energy in Equation 4c. There is also a wave contribution to the pressure in the form of a Bernoulli head (McWilliams et al. 2004). Ensemble closure models (e.g., Rascle et al. 2006) include the Coriolis-Stokes term but do not contain the vortex force, as it disappears when Equation 4a is averaged.

The LES models replicate features observed in outdoor flows. For example, **Figure 5*b*** illustrates the unsteady meandering and merging of surface particles, which are commonly observed traits of Langmuir turbulence (notice that the Y junctions are associated with collisions of neighboring pairs of LCs). Simulations also predict low-order moments not yet adequately sampled by field observations; e.g., D'Asaro (2001) measures vertical velocity. The mean currents, momentum and scalar fluxes, turbulence variances, and eddy viscosity from OBL simulations with wave effects exhibit large differences from flat-wall boundary layers. LCs homogenize the currents, leading to negative bulk eddy viscosity K_m near the surface; this is an indicator of nonlocal mixing and transport (see **Figure 6**). The ordering of the variances $\langle v'^2 \rangle \approx \langle w'^2 \rangle > \langle u'^2 \rangle$ at $z/|h| \sim -0.15$ and a large subsurface maximum in $\langle w'^2 \rangle$ demonstrate that wave-current interactions modify the OBL in important ways compared to flat-wall boundary layers. Teixeira & Belcher (2002) analyzed rapid distortion solutions for a propagating wave and determined that Stokes drift, acting repetitively over many wave cycles, also leads to the same ordering of normal variances that is fundamentally different from shear flow $\langle u'^2 \rangle > \langle v'^2 \rangle > \langle w'^2 \rangle$.

The Coriolis-Stokes term modifies the ocean Ekman transport and leads to a return flow opposite in sign to the Stokes drift, as shown in **Figure 6**. Empirical wind and wave estimates indicate the Coriolis-Stokes effect is an appreciable influence on the mean Ekman current profile in the OBL over most of the globe, and especially in high latitudes with high winds (McWilliams et al. 2004, Polton et al. 2005). Also, Stokes production increases TKE; thus dissipation near the surface is higher than law-of-the-wall scaling (McWilliams et al. 1997, Sullivan et al. 2007).

LES models predict that scalar heat flux and mixed-layer depth are enhanced by the vortex force. McWilliams et al. (1997), Skyllingstad et al. (2000), and Sullivan et al. (2007) all report that the maximum entrainment flux $\langle w'\theta' \rangle$ increases by a factor of two to five with vortex force. Skyllingstad (2005) interpreted the change as an indirect effect, i.e., as a consequence of LC momentum redistribution causing higher shear at the base of the OBL. LCs can excite gravity waves in the thermocline (Chini & Leibovich 2003, Polton et al. 2008), suggesting that they are depth filling and that they likely play a role in the entire OBL. The limited observational studies have yet to fully detect these changes. Gargett & Wells (2004) found LC depth filling, but in shallow water, whereas Thorpe et al. (2003a) and Weller & Price (1988) found no direct role for LCs in mixing near the base of an ∼[40–60] m deep layer.

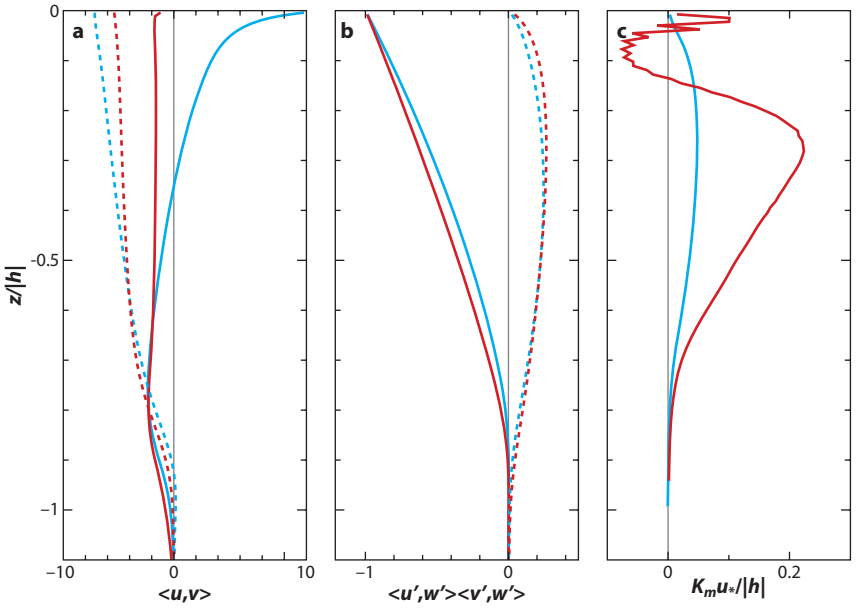

Figure 6

Comparison of (*a*) currents $\langle u, v\rangle/u_{*0}$, (*b*) vertical momentum fluxes $\langle u'w', v'w'\rangle/u_{*0}^2$, and (*c*) momentum eddy viscosity $K_m u_{*0}/|b|$ for simulations with (*red lines*) and without (*blue lines*) wave-current interactions. In panels *a* and *b*, the *u* and *v* components are indicated by solid and dashed lines, respectively (Sullivan et al. 2007). Figure used with permission of Cambridge University Press.

McWilliams et al. (1997) introduced the turbulent Langmuir number

$$La_t = \sqrt{u_{*0}/u^{St}} \tag{5}$$

as a bulk measure of the relative importance of shear and Stokes forcing. Li et al. (2005) investigated a wide parameter space spanned by shear, Stokes, and buoyancy forcing and concluded that most often the wind-driven OBL is dominated by Langmuir turbulence with $La_t \approx 0.3$ or less. Harcourt & D'Asaro (2007) and Li et al. (2005) emphasized that La_t is a single bulk measure and that other wave scales play a role in the Langmuir turbulence regime, notably the *e*-folding depth of the Stokes profile relative to the OBL depth d^{St}/h. Harcourt & D'Asaro (2007) reported that the magnitude and location of the maximum vertical velocity variance depend on $u^{St}(z)$ and wave age. The vertical structure of the Stokes drift profile was also emphasized by Gargett & Wells (2004), who noted that the finite-depth correction to Stokes drift is significant. Grant & Belcher (2009) found the variance profiles to be insensitive to d^{St}/h variations in the range 0.09–0.27 with an exponential Stokes profile. Better quantification of the wave field state, i.e., the wave age, wind-wave orientation, as well as the usual wave-height (energy) spectrum, along with simultaneous measurements of wind stress, is required to make consistent observation-model comparisons (measurements of breaking statistics are also needed).

Several aspects of the LES predictions invite further numerical evaluation and detailed experimental testing. First, the asymptotic CL model described above has no feedback from currents to waves in the leading-order wave dynamics. However, if observed waves are used to compute Stokes drift, this coupling is accounted for. Transient wave groups (Gargett & Wells 2004, Smith 1998) and wave breaking generate time-varying Stokes drift (Melville 1996, Phillips 2002), which is not incorporated into the CL equation set. Work by Zhou (1999) and Kawamura (2000) indicates that

the CL equations are a valid approximation for a fast moving monochromatic wave. Tsai & Hung (2007) developed a coupled wave-current numerical model with no breaking that is applicable to short waves in which the CL approximation is perhaps least valid.

3.2. Breaking Waves

Gravity waves are particularly important because they break intermittently. In the open ocean, the onset of breaking is a random process likely linked to the local winds, wave-wave and wave-current interactions, and the group structure of the surface wave field (Melville 1996). Wave breaking induces transient airflow separation, halts wave growth, sporadically injects momentum into the water column (Banner & Peirson 1998, Donelan 1998, Melville et al. 2002), and at sufficiently high wind speeds controls air-sea gas fluxes (Wanninkhof et al. 2009).

3.2.1. Current and turbulence generation. The dominant role of wave breaking for current generation is advocated by Donelan (1998) who showed self-consistency between waveform drag τ_w and measurements of wind stress τ_a using a statistical wave model. Over a broad wave-age range, $0.2 < c_p/U_a < 1.2$, the ratio $\tau_w/\tau_a \geq 0.95$; i.e., the majority of wind momentum is converted into waveform stress and deposited locally to currents with only a small fraction, 5%, propagated away by waves. [A similar analysis shows the same partitioning for energy flux. By definition, 100% of the momentum and energy fluxes is passed directly to the currents in homogeneous wind-wave equilibrium, $c_p/U_a \to 1.2$.] Intermittent wave breaking is thus the dominant process for transferring momentum to currents at wind speeds above 8 m s^{-1} (Donelan 1998). Makin et al. (1995, their figure 4) used a similar statistical wave model and found that τ_w is concentrated at wavelengths in the range 5 cm $< \lambda <$ 10 m for fully developed seas at $U_a = 10$ m s^{-1}. The range shifts toward larger scales for smaller wave age.

The breaking-dissipation sink term in statistical wave models is a highly parameterized function with almost no direct observational validation (Donelan 2001, Komen et al. 1994). Melville & Matusov (2002) attempted to quantify breaking by measuring the momentum and energy transfer from individual breaking events. They used airborne imagery of the sea surface to track active breakers and digitized the movies to determine $\Lambda(c)dc$, i.e., the average length of breaking fronts per unit area of sea surface traveling in the range $(c, c + dc)$, first introduced by Phillips (1985). Momentum and energy flux from waves to currents are the high-order moments $c^4\Lambda(c)$ and $c^5\Lambda(c)$, respectively. They found that $\Lambda(c)$ varies exponentially with the momentum and energy fluxes peaking at intermediate-scale waves $c \sim \mathcal{O}(4$ m s$^{-1})$; i.e., $\lambda \sim 10$ m. The observed contributions to fluxes from waves with $c < 1$ m s^{-1} are small.

Gemmrich et al. (2008) used a similar video technique as Melville & Matusov (2002) but acquired images closer to the water surface, $z \sim 10$ m, from cameras mounted on R/V FLIP (a floating instrument platform). Their results for breaking probability show a dependence on wave age and c/c_p: For wind-driven waves, breakers are found across the entire range, $c/c_p = [0.1–1]$, with the highest probability near $0.4c_p$; for wind-wave equilibrium, breaking is confined to a narrow range, $c/c_p = [0.1–0.5]$, with a peak near $0.2c_p$. Their analysis also indicates white-capping breakers likely account for [11–17]% of the momentum flux. Gemmrich et al. (2008) suggested that the missing momentum and energy are in small-scale breakers with $c < 1.5$ m s^{-1}. Small temperature changes generated by the overturning of these small-scale breakers can be detected using infrared techniques (Jessup & Phadnis 2005) and thus fill in missing information about breaking statistics over the entire range of scales.

The clearest evidence for the effect of wave breaking on the OBL surface layer remains the data sets collected by Terray et al. (1999) and Drennan et al. (1996). Their measurements of

kinetic-energy dissipation ε under conditions of strong wind forcing show a layer of enhanced dissipation exceeding stationary wall-layer values by one to two orders of magnitude. The dissipation rate has a three-layer z structure: Within one significant wave height of the surface, ε is large and nearly constant; below this zone ε decays as z^{-2} and finally transitions into conventional wall-layer scaling $\varepsilon \sim z^{-1}$ at deeper depths. The total energy flux into the water is an order of magnitude larger than the usual wall-layer estimate $\rho_o u_{*0}^3/2$ and depends strongly on wave age.

To examine the consequences of intermittent wave breaking and vortex force, we developed an LES model with both effects (Sullivan et al. 2007). In this LES, the constant stress upper-boundary condition is replaced by a sum of randomly distributed compact impulses $\sum \mathbf{A}(\mathbf{x}, t)$ first tested in a DNS of Couette flow (Sullivan et al. 2004). The space-time attributes of an individual impulse $\mathbf{A}(\mathbf{x}, t)$ are designed to match field (Melville & Matusov 2002) and laboratory observations (Melville et al. 2002) of breaking waves and the mean fluxes of momentum and energy. Schematically, the LES equations for resolved-scale momentum (Equation 4a) and subgrid-scale energy (Equation 4c) become

$$\frac{\partial \tilde{\mathbf{u}}}{\partial t} = \ldots + \sum_{i=1}^{n} \mathbf{A}^{(i)}, \quad \frac{\partial e}{\partial t} = \ldots + \sum_{i=1}^{n} W^{(i)}, \tag{6}$$

where breaker work $W \sim \mathbf{c} \bullet \mathbf{A}$.

As expected, the inclusion of wave effects elevates the overall TKE (and hence dissipation) in the OBL, especially in the near-surface region. ε increases over law-of-the-wall scaling by nearly two orders of magnitude, with the increase from breaker work an order of magnitude larger than from Stokes production. Below the region of enhanced dissipation, $z/|b| < -0.1$, simulations with vortex force and breaking are broadly similar to vortex-force-only simulations. However, for growing wave fields, $c_p/u_{*a} \approx 19$, breakers can combine with vortex force to instigate a deep, strong, intermittent downwelling jet that increases the material entrainment rate at the base of the layer. Essentially, breaker vorticity concentrated at the surface catalyzes the CL2 instability. These wave effects on the boundary layer are greater for smaller wave ages and higher mean wind speeds. Noh et al. (2004) also examined this regime, but with a representation of wave breaking collapsed to the water surface using the Craig (2005) boundary condition.

3.2.2. Bubbles. Subsurface bubble clouds generated by breaking waves are a powerful signature of wind-wave-current coupling. Bubbles range in size from tens of micrometers to centimeters with void fractions up to 10% (Deane & Stokes 2002). They change the optical properties of water (Terrill et al. 2001), alter sound transmission (Melville 1996), and most importantly are a first-order effect on air-sea gas flux especially at high winds (D'Asaro & McNeil 2007, Wanninkhof et al. 2009). Bubbles move under the action of background turbulence, intermittent wave-breaking penetrations, and coherent LCs. LCs are particularly effective in depositing bubbles to deeper depths against their natural tendency to rise [e.g., D'Asaro & McNeil (2007) found bubbles at $z = -10$ m]. The greatest uncertainty in developing bubble models is in the representation of the unsteady currents that disperse bubbles from their surface sources (Thorpe et al. 2003b). Bubbles can also have a meaningful dynamical effect: Large void fractions near the surface create patches of stable stratification, which can hinder vertical mixing. The incorporation of dynamical bubble models into LES with wave effects is an important area for future research.

3.3. Oceanic Boundary Layers with Inertial Currents and Surface Waves

The wave fields and turbulence that mix the OBL frequently coexist with much larger-scale inertial currents initiated by the passage of intermittent storms, cold fronts, rapidly moving lows, and in

particular hurricanes (D'Asaro 1985, Large & Crawford 1995, Price et al. 1994, Sanford et al. 2007). A resonant condition in the ocean is set up when storms generate large-amplitude wind stress that rotates with the surface currents over an extended period, as discussed by Ferrari & Wunsch (2009). In mid-latitudes, the inertial current timescale $1/f = \mathcal{O}(10^4\ \mathrm{s})$ is long compared to turbulence and surface waves.

OBL inertial currents are widespread (Stockwell et al. 2004) and are considered important because they alter sea-surface temperature, a key air-sea coupling variable (Emanuel 2004). Large current gradients at the base of the stably stratified thermocline lower the local Richardson number and promote Kelvin-Helmholtz instabilities and turbulence, which enhance the vertical transport of momentum and scalars. Theoretical models for the OBL currents in a wind-driven inertial regime adopt ensemble-average Ekman equations with time-dependent forcing (e.g., Gill 1982, chapter 9.3):

$$\frac{\partial u}{\partial t} - f\,v = -\frac{\partial \langle u'w' \rangle}{\partial z}, \tag{7a}$$

$$\frac{\partial v}{\partial t} + f\,u = -\frac{\partial \langle v'w' \rangle}{\partial z}. \tag{7b}$$

In these coupled equations, (u, v) are average currents and $\langle \mathbf{u}'w' \rangle$ are net turbulent fluxes of vertical momentum. No surface-wave effects are directly accounted for in these equations (wave influences might inadvertently be buried in the turbulence parameterization).

D'Asaro (1985) uses Equation 7 with an added damping term and predicts resonant inertial currents when the wind stress contains a frequency component near f. Crawford & Large (1995) also uses Equation 7 but employs a more complete model of the turbulent fluxes based on the K-profile parameterization scheme (Large et al. 1994). Their numerical experiments consider perfectly resonant forcing $\boldsymbol{\tau}_a = A(t)e^{-ift}$ with storm amplitude $A(t)$ and emphasize the importance of kinetic-energy transfer to the ocean through the stress-current correlation $\int \boldsymbol{\tau}_a \cdot \mathbf{u}\, dt$. For similar strength storms, episodic cooling events are only observed by Large & Crawford (1995) when the initial current state and wind stress are in phase. Skyllingstad et al. (2000) used LES to examine resonant and off-resonant wind forcing similar to Crawford & Large (1995), but also included relatively modest wave-forcing scenarios. They found that the greatest mixing occurs under resonance conditions with only minor enhancements due to surface-wave effects.

To investigate OBL dynamics with both inertial currents and vortex force, we designed an LES with realistic time-evolving hurricane wind forcing and a simple wave prescription: Hurricane wave fields are highly complex (Wright et al. 2001), and the wave model is designed to test solution sensitivity. For the experiments, we set $La_t = 0.3$ and wave age $= 0.6$, which fixes the parameters in an exponential Stokes drift profile. We used winds and stresses representative of Hurricane Frances (Zedler 2007) with a saturated drag coefficient $C_d \sim 1.5 \times 10^{-3}$ and a surface buoyancy forcing based on a relative humidity of 80% and temperature difference of 2.5 K between the water surface and the atmosphere. The time-varying wind, buoyancy, and wave forcing were applied to the top of the LES for a period of 60 h.

The LES results presented in **Figure 7** are intriguing. The statistics and structures between [0–20] h are similar to calculations with steady forcing; i.e., vortex force plays an important role in mixing currents and scalars. Between [30–40] h, the rapid turning of the winds on the storm's right-hand side induces potent inertial currents and strong resonance in the OBL. Over this time period, the OBL dynamics are dominated by entrainment, which further stresses the basic importance of turbulent mixing at stratified interfaces (Fernando 1991). At the time of maximum winds, the entrainment-to-surface flux ratio is ~ -10 without vortex force and ~ -12 with vortex force, i.e., at least a 20% increase. Thus surface-wave-current interaction, in these idealized

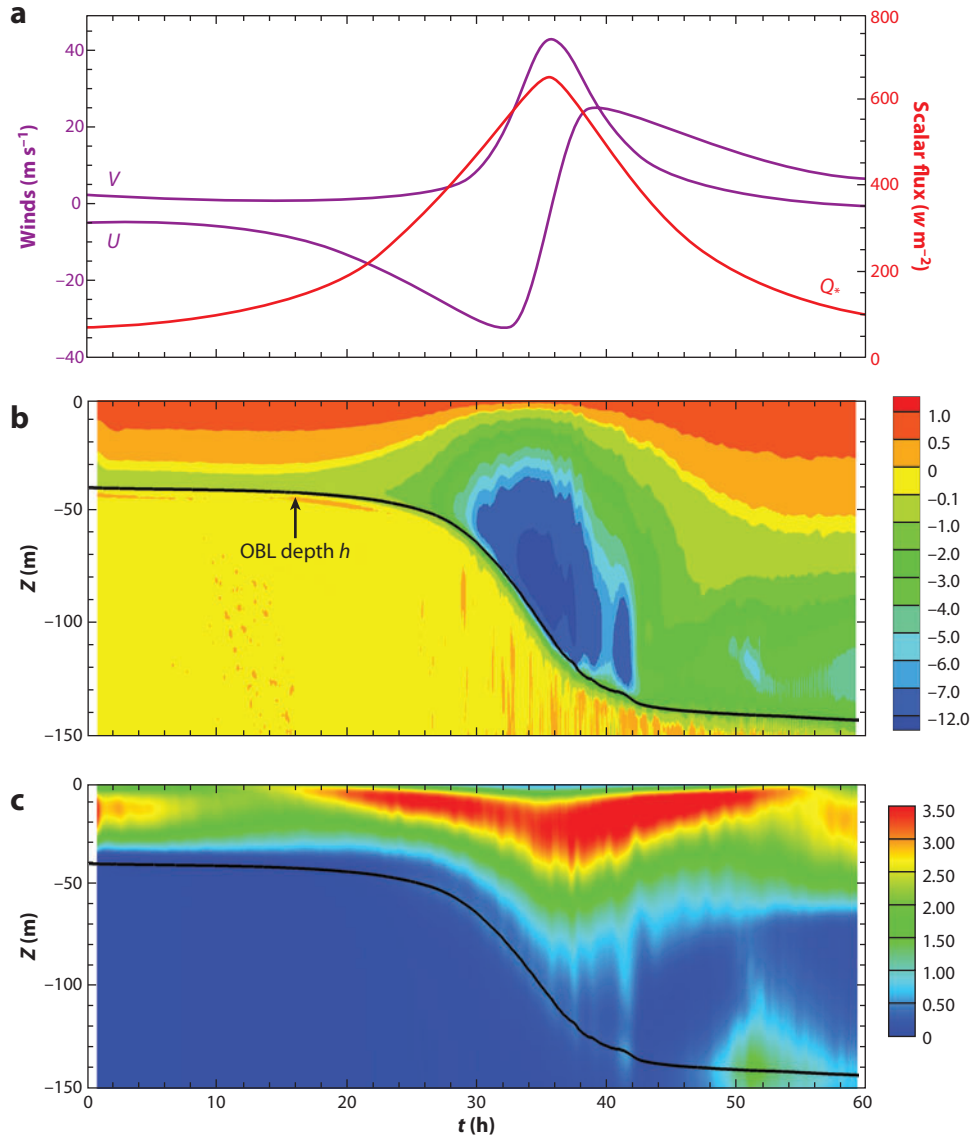

Figure 7

Vertical profiles of turbulent scalar flux and vertical velocity variance from a large-eddy simulation (LES) of an oceanic boundary layer (OBL) driven by Hurricane Frances winds and buoyancy with vortex force. The time variation of the wind (U, V) and buoyancy forcing Q_* are given in panel *a*. The LES domain is located on the right-hand (resonance) side of the storm, initially 55 km east and 700 km north of the storm's center. The storm propagates northward at 5.5 m s^{-1}. The total scalar flux $\langle w'\theta' \rangle / Q_*$ and vertical velocity variance $\langle w'^2 \rangle / u_{*0}^2$ are shown in panels *b* and *c*, respectively. The black line is the depth of the maximum vertical temperature gradient, which can be interpreted as the OBL depth. The mesh is 500 × 500 × 160 grid points, and the time step Δt varies from 15 s to 0.4 s over the length of the simulation. The total number of time steps is ~200,000.

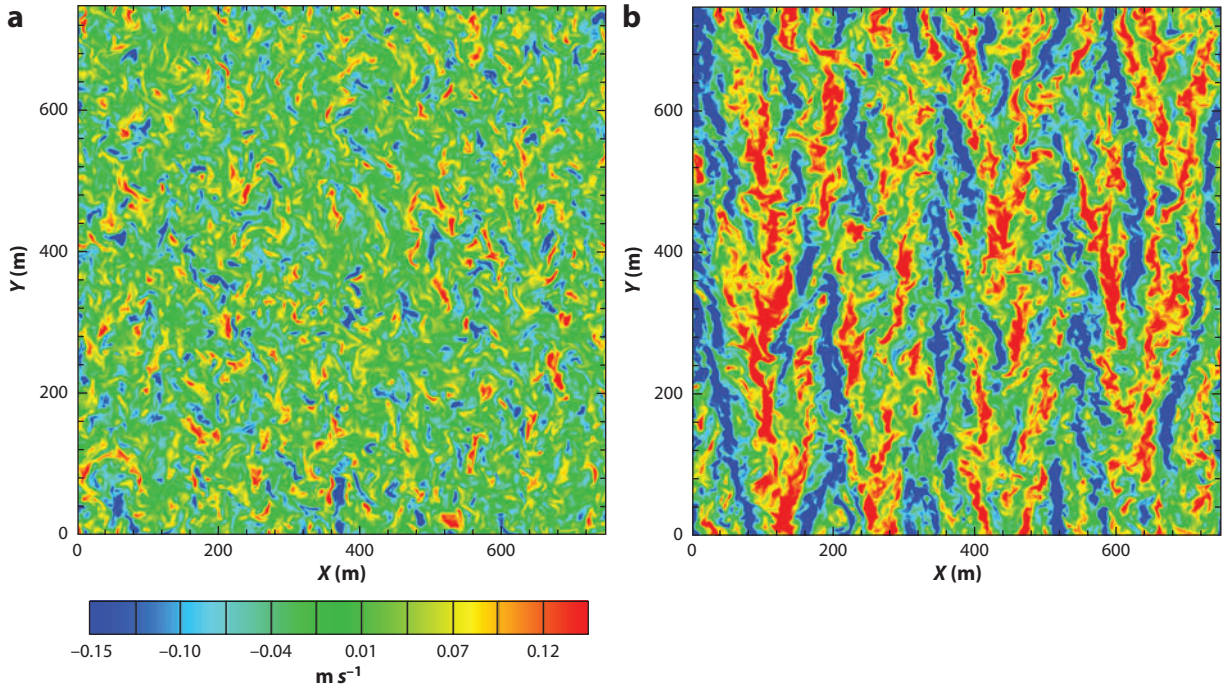

Figure 8

Visualization of the vertical velocity field in an x-y plane at $z = -30.0$ m at the time of maximum winds shown in **Figure 7**, $t \sim 35.3$ h. Panel *a* shows results from a large-eddy simulation with no vortex force, whereas panel *b* is a simulation with $La_t = 0.3$ and wave age $= 0.6$. At this simulation time, the wind and wave-propagation directions are south to north. In panel *b*, the elongated regions with $w < 0$ (*blue contours*) are the downwelling signatures of Langmuir circulations. The scale bar is in units of meters per second.

calculations, promotes cooling. Simulations with vortex force and resonant inertial currents induce deeper mixed layers, higher entrainment rates, and lower sea-surface temperatures. Also, the mean (u, v) currents are more uniformly mixed during the resonant period, with their phase relationship slightly altered by the presence of vortex force. In the surface-layer region, the vertical velocity ratio $\langle w'^2 \rangle / u_{*0}^2$ reaches 3.5, similar to predictions with steady nonresonant wind forcing (McWilliams et al. 1997, Skyllingstad & Denbo 1995). At the time of maximum winds, prominent Langmuir cells are visible over the OBL depth, with downwelling speeds exceeding 20 cm s^{-1} (see **Figure 8**).

3.4. Parameterization of Wave Effects in the Oceanic Boundary Layer

There is a growing appreciation of the dynamical importance of surface waves and hence a need to incorporate wave effects (wave breaking, bubbles, and wave-current interactions) into simple 1D column models for use in climate prediction and regional ocean mesoscale codes. Belcher et al. (2008), using ECMWF reanalysis products, found that $La_t < 1$ for the global ocean; hence the OBL is most often in the Langmuir turbulence regime accompanied with some level of wave breaking. The bulk wave influences to be modeled can be split into two groups: (*a*) elevated mixing and dissipation in the near-surface region caused by wave breaking and (*b*) deeper penetration into the thermocline and more uniformly mixed interiors caused by vortex forces. Parameterization of these effects is proceeding at varying levels of completeness. The inclusion of breaking waves

was discussed by Craig (2005), who represents breaking waves in his TKE closure by a surface flux $F_o = \alpha u_{*0}^3$; Terray et al. (1999) showed how α varies with wave age. Umlauf & Burchard (2003) can also predict the enhanced turbulent dissipation rates using a two-equation turbulence closure. Stokes production of TKE was included by Kantha & Clayson (2004), and Rascle et al. (2006) incorporated Stokes production, a Coriolis-Stokes term, and parameterized wave breaking in their ensemble average closures. In these TKE modeling approaches, a local eddy viscosity closure is used, i.e., $\tau \sim -\nu_t \partial u/\partial z$, which, as shown in **Figure 6**, is incapable of representing nonlocal mixing induced by Langmuir cells. McWilliams & Sullivan (2000) and Smyth et al. (2002) recently attempted to account for both mixed-layer depth changes and nonlocal mixing by Langmuir cells using K-profile parameterization (Large et al. 1994). They included a nonlocal counter-gradient term similar to the approach used for convective ABLs.

ECMWF: European Centre for Medium-Range Weather Forecasts

4. SUMMARY

Surface gravity waves strongly couple to adjacent winds and currents. This invalidates the prevailing paradigm for turbulent boundary layers, e.g., that near-boundary flow structure be consistent with a thin viscous-diffusive sublayer inside a surface layer exhibiting Monin-Obukhov similarity statistics (i.e., the law of the wall). The wavy interface is usually rough and often fragmented, and its dynamical evolution is not independent of other air and water flows, especially for wave generation and dissipation. This review addresses many of the processes involved in wind-wave-current interaction, although a fully integrated view has not yet been achieved. Waves grow from atmospheric pressure forces on the perturbed surface and provide drag to the airflow. Winds in the lower atmosphere are pumped up by the wave motions and affect vertical fluxes to and from the surface. Wave breaking dissipates wave energy, generates spray and bubbles, and injects energy and momentum into currents. Wave-induced Stokes drift affects the OBL through vortex force and material advection, giving rise to widespread LCs. Under some conditions, surface-wave influences are felt throughout the planetary boundary layers. Because accurate, extensive outdoor measurements of waves and turbulence are and will remain difficult, LES is an important tool for phenomenological discovery and quantification, albeit vulnerable to uncertainty in its subgrid-scale modeling.

5. OUTLOOK

Although surface waves and turbulent boundary layers are mature scientific subjects, we are in the midst of rapid progress in understanding their mutual relationships. We foresee the following directions as fruitful ones in coming years: (*a*) complex wave surfaces in ABL and OBL LES; (*b*) coupled wind-wave and wave-current models; (*c*) OBL and ABL mixing parameterizations with wave effects; (*d*) wave-breaking structure and statistical distributions; (*e*) disequilibrium, misaligned wind-wave conditions; (*f*) wave and turbulence mechanics in high winds (e.g., hurricanes); and (*g*) bubbles and spray.

DISCLOSURE STATEMENT

The authors are not aware of any affiliations, memberships, funding, or financial holdings that might be perceived as affecting the objectivity of this review.

ACKNOWLEDGMENTS

We wish to acknowledge the efforts of coauthors and collaborators Ken Melville, Chin-Hoh Moeng, Juan Restrepo, and Emily Lane who cheerfully made contributions to our work over many years. Stephen Belcher and coworkers shared their unpublished work with us. We also thank Michael Black, Fabrice Veron, Mark Donelan, and Stephen Monismith who allowed us to display their results. Regretfully, we are unable to include the many important contributions of numerous colleagues in an article of finite length, and give our sincere apologies. The long-term support and commitment to surface waves from the Physical Oceanography and Marine Meteorology Programs of the Office of Naval Research helped make this research possible. The National Center for Atmospheric Research is sponsored by the National Science Foundation.

LITERATURE CITED

Alves JGM, Banner ML, Young IR. 2003. Revisiting the Pierson-Moskowitz asymptotic limits for fully developed wind waves. *J. Phys. Oceanogr.* 33:1301–23

Banner ML, Melville WK. 1976. On the separation of airflow over water waves. *J. Fluid Mech.* 77:825–42

Banner ML, Peirson WL. 1998. Tangential stress beneath wind-driven air-water interfaces. *J. Fluid Mech.* 364:115–45

Baumert HZ, Simpson J, Sündermann J, eds. 2005. *Marine Turbulence: Theories, Observations, and Models*. Cambridge, UK: Cambridge Univ. Press

Belcher SE, Grant ALM, Hanley KE, Sullivan PP. 2008. Surface wave processes in air-sea interaction. *Proc. ECMWF Workshop Ocean-Atmos. Interact.*, pp. 75–82

Belcher SE, Hunt JCR. 1998. Turbulent flow over hills and waves. *Annu. Rev. Fluid Mech.* 30:507–38

Bement AL. 2007. Cyberinfrastructure vision for 21st century discovery. *NSF 07-28*, NSF Cyberinfrastruct. Council; **http://www.nsf.gov/pubs/2007/nsf0728/index.jsp**

Black P, D'Asaro E, Drennan W, French J, Niiler P, et al. 2007. Air-sea exchange in hurricanes: synthesis of observations from the Coupled Boundary Layers Air-Sea Transfer experiment. *Bull. Am. Meteorol. Soc.* 88:357–74

Bye JAT, Jenkins AD. 2006. Drag coefficient reduction at very high wind speeds. *J. Geophys. Res.* 111:C03024

Chen SS, Price JF, Zhao W, Donelan MA, Walsh EJ. 2007. The CBLAST-hurricane program and the next-generation fully coupled atmosphere-wave-ocean models for hurricane research and prediction. *Bull. Am. Meteorol. Soc.* 88:311–17

Chini GP, Leibovich S. 2003. Resonant Langmuir-circulation internal-wave interaction. Part 1. Internal wave reflection. *J. Fluid Mech.* 495:35–55

Craig P. 2005. Modeling turbulence generation by breaking waves. See Baumert et al. 2005, pp. 273–76

First derivation of vortex force.

Craik A, Leibovich S. 1976. A rational model for Langmuir circulations. *J. Fluid Mech.* 73:401–26

Crawford GB, Large WG. 1995. A numerical investigation of resonant inertial response of the ocean to wind forcing. *J. Phys. Oceanogr.* 26:873–91

Csanady GT. 2001. *Air-Sea Interaction: Laws and Mechanisms*. Cambridge, UK: Cambridge Univ. Press

D'Asaro E. 1985. The energy flux from the wind to near-inertial motion in the surface mixed layer. *J. Phys. Oceanogr.* 15:1043–59

D'Asaro E. 2001. Turbulent vertical kinetic energy in the ocean mixed layer. *J. Phys. Oceanogr.* 31:3530–37

Gas flux measurements in high winds.

D'Asaro E, McNeil C. 2007. Air-sea gas exchange at extreme wind speeds measured by autonomous oceanographic floats. *J. Mar. Syst.* 66:92–109

Deane GB, Stokes MD. 2002. Scale dependence of bubble creation mechanisms in breaking waves. *Nature* 418:839–44

Donelan MA. 1998. Air-water exchange processes. In *Physical Processes in Lakes and Oceans*, ed. J Imberger, pp. 19–36. Coast. Estuar. Stud. 54. Washington, DC: Am. Geophys. Union

Donelan MA. 1999. Wind-induced growth and attenuation of laboratory waves. *Proc. Inst. Math. Appl. (UK) Conf. Wind-Over-Wave Couplings*, pp. 183–94. Oxford, UK: Oxford Univ. Press

Donelan MA. 2001. A nonlinear dissipation function due to wave breaking. *Proc. Workshop Ocean Wave Forecast.*, pp. 87–94. Reading, UK: Eur. Center Medium Range Weather Forecast.
Donelan MA, Babanin AV, Young IR, Banner ML. 2006. Wave-follower field measurements of the wind-input spectral function. Part II: parameterization of the wind input. *J. Phys. Oceanogr.* 36:1672–89
Donelan MA, Dobson FW. 2001. The influence of swell on the drag. See Jones & Toba 2001, pp. 181–89
Donelan MA, Haus BK, Reul N, Plant WJ, Stiassnie M, et al. 2004. On the limiting aerodynamic roughness of the ocean in very strong winds. *Geophys. Res. Lett.* 31:L18306
Drennan WM, Donelan MA, Terray EA, Katsaros KB. 1996. Oceanic turbulence dissipation measurements in SWADE. *J. Phys. Oceanogr.* 26:808–15
Edson J, Crawford T, Crescenti J, Farrar T, French J, et al. 2007. The coupled boundary layers and air-sea transfer experiment in low winds (CBLAST-Low). *Bull. Am. Meteorol. Soc.* 88:342–56
Eifler W. 2005. The near-surface boundary layer. See Baumer et al. 2005, pp. 250–72
Emanuel K. 2004. Tropical cyclone energetics and structure. In *Atmospheric Turbulence and Mesoscale Meteorology*, ed. E Fedorovich, R Rotunno, B Stevens, pp. 165–91. Cambridge, UK: Cambridge Univ. Press
Fairall CW, Bradley EF, Hare JE, Grachev AA, Edson JB. 2003. Bulk parameterization of air-sea fluxes: updates and verification for the COARE algorithm. *J. Clim.* 16:571–91
Fernando HJS. 1991. Turbulent mixing in stratified fluids. *Annu. Rev. Fluid Mech.* 23:455–93
Ferrari R, Wunsch C. 2009. Ocean circulation kinetic energy: reservoirs, sources, and sinks. *Annu. Rev. Fluid Mech.* 41:253–82
Gargett A, Wells JR. 2004. Langmuir turbulence in shallow water. Part 1. Observations. *J. Fluid Mech.* 576:27–61
Gemmrich JR, Banner ML, Garrett C. 2008. Spectrally resolved energy dissipation rate and momentum flux of breaking waves. *J. Phys. Oceanogr.* 38:1296–312
Gent PR, Taylor PA. 1977. A note on 'separation' over short wind waves. *Boundary-Layer Meteorol.* 11:105–28
Gill AE. 1982. *Atmosphere-Ocean Dynamics*. New York: Academic
Graber HC, Terray EA, Donelan MA, Drennan WM, Van Leer JC. 2000. ASIS—a new air-sea interaction spar buoy: design and performance at sea. *J. Atmos. Oceanic Technol.* 17:708–20
Grachev AA, Fairall CW. 2001. Upward momentum transfer in the marine boundary layer. *J. Phys. Oceanogr.* 31:1698–711
Grachev AA, Fairall CW, Hare JE, Edson JB, Miller SD. 2003. Wind stress vector over ocean waves. *J. Phys. Oceanogr.* 33:2408–29
Grant ALM, Belcher SE. 2009. Characteristics of Langmuir turbulence in the ocean mixed layer. *J. Phys. Oceanogr.* In press
Hanley KE. 2008. *A global perspective of wind-wave interaction and the distribution of wave momentum*. PhD thesis, Univ. Reading
Hanley KE, Belcher SE. 2008. Wave-driven wind jets in the marine atmospheric boundary layer. *J. Atmos. Sci.* 65:2646–60
Harcourt RR, D'Asaro EA. 2007. Large-eddy simulation of Langmuir turbulence in pure wind seas. *J. Phys. Oceanogr.* 38:1542–62
Hatlee SC, Wyngaard JC. 2007. Improved subfilter-scale models from the HATS field data. *J. Atmos. Sci.* 64:1694–705
Hristov T, Friehe C, Miller S. 1998. Wave-coherent fields in air flow over ocean waves: identification of cooperative behavior buried in turbulence. *Phys. Rev. Lett.* 81:5245–48
Hristov T, Miller SD, Friehe C. 2003. Dynamical coupling of wind and ocean waves through wave-induced air flow. *Nature* 422:55–58
Janssen PAEM. 1991. Quasi-linear theory of wind-wave generation applied to wave forecasting. *J. Phys. Oceanogr.* 21:1631–42
Janssen PAEM. 2008. Progress in ocean wave forecasting. *J. Comp. Phys.* 227:3572–94
Jessup AT, Phadnis KR. 2005. Measurement of the geometric and kinematic properties of microscale breaking waves from infrared imagery using a PIV algorithm. *Meas. Sci. Technol.* 16:1961–69
Jones ISF, Toba Y. 2001. *Wind Stress Over the Ocean*. Cambridge, UK: Cambridge Univ. Press
Kantha LH, Clayson CA. 2004. On the effect of surface gravity waves on mixing in the oceanic mixed layer. *Ocean Model.* 6:101–24

Laboratory measurements showing drag saturation at high winds.

Observations of critical-layer dynamics over the ocean.

Kawamura T. 2000. Numerical investigation of turbulence near a sheared air-water interface. Part 2: interaction of turbulent shear flow with surface waves. *J. Mar. Sci. Technol.* 5:161–75

Kihara N, Hanazaki H, Mizuya T, Ueda H. 2007. Relationship between airflow at the critical height and momentum transfer to the traveling waves. *Phys. Fluids* 19:015102

Komen GJ, Cavaleri L, Donelan M, Hasselmann K, Hasselmann S, Janssen PAEM. 1994. *Dynamics and Modelling of Ocean Waves*. Cambridge, UK: Cambridge Univ. Press

Lane EM, Restrepo JM, McWilliams JC. 2007. Wave-current interaction: a comparison of radiation-stress and vortex-force representations. *J. Phys. Oceanogr.* 37:1122–41

Large WG, Crawford G. 1995. Observations and simulations of upper-ocean response to wind events during the ocean storms experiment. *J. Phys. Oceanogr.* 25:2831–52

Large WG, McWilliams JC, Doney SC. 1994. Oceanic vertical mixing: a review and a model with a nonlocal boundary layer parameterization. *Rev. Geophys.* 32:363–403

Large WG, Pond S. 1981. Open ocean flux measurements in moderate to strong winds. *J. Phys. Oceanogr.* 11:324–36

Leibovich S. 1983. The form and dynamics of Langmuir circulations. *Annu. Rev. Fluid Mech.* 15:391–427

Li M, Garrett C, Skyllingstad E. 2005. A regime diagram for classifying turbulent large eddies in the upper ocean. *Deep-Sea Res. I* 52:259–78

Lighthill J. 1978. *Waves in Fluids*. Cambridge, UK: Cambridge Univ. Press

Lighthill MJ. 1962. Physical interpretation of the mathematical theory of wave generation by wind. *J. Fluid Mech.* 14:385–98

Lin I, Liu WT, Wu CC, Wong GTF, Hu C, et al. 2003. New evidence for enhanced ocean primary production triggered by tropical cyclone. *Geophys. Res. Lett.* 30:L1718

Makin VK. 2008. On the possible impact of a following-swell on the atmospheric boundary layer. *Boundary-Layer Meteorol.* 129:469–78

Makin VK, Kudryavtsev VN, Mastenbroek C. 1995. Drag of the sea surface. *Boundary-Layer Meteorol.* 73:159–82

Mastenbroek C, Makin VK, Garat MH, Giovanangeli JP. 1996. Experimental evidence of the rapid distortion of turbulence in the air flow over water waves. *J. Fluid Mech.* 318:273–302

McWilliams JC. 1996. Modeling the oceanic general circulation. *Annu. Rev. Fluid Mech.* 28:215–48

Demonstrates the importance of Coriolis-Stokes transport in the OBL.

McWilliams JC, Restrepo JM. 1999. The wave-driven ocean circulation. *J. Phys. Oceanogr.* 29:2523–40

McWilliams JC, Restrepo JR, Lane EM. 2004. An asymptotic theory for the interaction of waves and currents in shallow coastal water. *J. Fluid Mech.* 511:135–78

McWilliams JC, Sullivan PP. 2000. Vertical mixing by Langmuir circulations. *Spill Sci. Technol. Bull.* 6:225–37

Introduced concept of Langmuir turbulence.

McWilliams JC, Sullivan PP, Moeng CH. 1997. Langmuir turbulence in the ocean. *J. Fluid Mech.* 334:1–30

Meirink JF, Makin VK. 2001. Modelling low-Reynolds-number effects in the turbulent air flow over water waves. *J. Fluid Mech.* 415:155–74

Melville WK. 1996. The role of wave breaking in air-sea interaction. *Annu. Rev. Fluid Mech.* 28:279–321

Melville WK, Matusov P. 2002. Distribution of breaking waves at the ocean surface. *Nature* 417:58–63

Melville WK, Veron F, White CJ. 2002. The velocity field under breaking waves: coherent structures and turbulence. *J. Fluid Mech.* 454:203–33

Miles JW. 1957. On the generation of surface waves by shear flow, part I. *J. Fluid Mech.* 3:185–204

Miller SD. 1999. *The structure of turbulent and wave-induced wind fields over open-ocean waves*. PhD thesis, Univ. Calif. Irvine

Moeng CH. 1984. A large-eddy simulation model for the study of planetary boundary-layer turbulence. *J. Atmos. Sci.* 41:2052–62

Moin P, Mahesh K. 1998. Direct numerical simulation: a tool in turbulence research. *Annu. Rev. Fluid Mech.* 30:539–78

Munk W. 2009. An inconvenient sea truth: spread, steepness, and skewness of surface slopes. *Annu. Rev. Mar. Sci.* 1:377–415

Noh Y, Min HS, Raasch S. 2004. Large eddy simulation of the ocean mixed layer: the effects of wave breaking and Langmuir circulation. *J. Phys. Oceanogr.* 34:720–35

Ocampo-Torres FJ, Donelan MA, Merzi N, Jia F. 1994. Laboratory measurements of mass transfer of carbon dioxide and water vapour for smooth and rough conditions. *Tellus Ser. B* 46:16–32

Peirson WL, Garcia AW. 2008. On the wind-induced growth of slow water waves of finite steepness. *J. Fluid Mech.* 608:243–74

Phillips OM. 1977. *Dynamics of the Upper Ocean*. Cambridge, UK: Cambridge Univ. Press

Phillips OM. 1985. Spectral and statistical properties of the equilibrium range in wind-generated gravity waves. *J. Fluid Mech.* 156:505–31

Phillips WRC. 2002. Langmuir circulations beneath growing or decaying surface waves. *J. Fluid Mech.* 469:317–42

Polton JA, Lewis DM, Belcher SE. 2005. The role of wave-induced Coriolis-Stokes forcing on the wind-driven mixed layer. *J. Phys. Oceanogr.* 35:444–57

Polton JA, Smith JA, MacKinnon JA, Tejada-Martinez AE. 2008. Rapid generation of high frequency internal waves beneath a wind wave forced oceanic surface mixed layer. *Geophys. Res. Lett.* 35:L13602

Pope SB. 2000. *Turbulent Flows*. Cambridge, UK: Cambridge Univ. Press

Powell MD, Vickery PJ, Reinhold TA. 2003. Reduced drag coefficient for high wind speeds in tropical cyclones. *Nature* 422:279–83

Price JF, Sanford T, Forristall G. 1994. Forced stage response to a moving hurricane. *J. Phys. Oceanogr.* 24:233–60

Rascle N, Ardhuin F, Terray EA. 2006. Drift and mixing under the ocean surface: a coherent one-dimensional description with application to unstratified conditions. *J. Geophys. Res.* 111:C03016

Reul N, Branger H, Giovanangeli JP. 2007. Air flow structure over short-gravity breaking waves. *Boundary-Layer Meteorol.* 126:477–505

Sanford TB, Price JF, Girton JB, Webb DC. 2007. Highly resolved observations and simulations of the ocean response to a hurricane. *Geophys. Res. Lett.* 34:L13604

First measurements of current profiles beneath a hurricane.

Shen L, Zhang X, Yue DKP, Triantafyllou MS. 2003. Turbulent flow over a flexible wall undergoing a streamwise travelling wave motion. *J. Fluid Mech.* 484:197–221

Skyllingstad E. 2005. Langmuir circulation. See Baumert et al. 2005, pp. 277–82

Skyllingstad ED, Denbo DW. 1995. An ocean large-eddy simulation of Langmuir circulations and convection in the surface mixed layer. *J. Geophys. Res.* 100:8501–22

Skyllingstad ED, Smyth WD, Crawford GB. 2000. Resonant wind-driven mixing in the ocean boundary layer. *J. Phys. Oceanogr.* 30:1866–90

Smedman A, Högström U, Bergström H, Rutgersson A. 1999. A case study of air-sea interaction during swell conditions. *J. Geophys. Res.* 104:25833–51

Smedman A, Tjernström M, Högström U. 1994. The near-neutral marine atmospheric boundary layer with no surface shearing stress: a case study. *J. Atmos. Sci.* 51:3399–411

Smith JA. 1998. Evolution of Langmuir circulation during a storm. *J. Geophys. Res.* 103:12649–68

Smyth WD, Skyllingstad ED, Crawford GB, Wijesekera H. 2002. Nonlocal fluxes and Stokes drift effects in the K-profile parameterization. *Ocean Dyn.* 52:104–15

Snyder RL, Dobson FW, Elliott JA, Long RB. 1981. Array measurements of atmospheric pressure fluctuations above surface gravity waves. *J. Fluid Mech.* 102:1–59

Stevens B, Lenschow DH, Vali G, Gerber H, Bandy A, et al. 2003. Dynamics and chemistry of marine stratocumulus: DYCOMS-II. *Bull. Am. Meteorol. Soc.* 84:579–93

Stockwell RG, Large WG, Milliff RF. 2004. Resonant inertial oscillations in moored buoy ocean surface winds. *Tellus* 56A:536–47

Sullivan PP, Edson JB, Hristov T, McWilliams JC. 2008. Large eddy simulations and observations of atmospheric marine boundary layers above non-equilibrium surface waves. *J. Atmos. Sci.* 65:1225–45

Large-eddy simulation of wave-driven winds.

Sullivan PP, Horst TW, Lenschow DH, Moeng CH, Weil JC. 2003. Structure of subfilter-scale fluxes in the atmospheric surface layer with application to large-eddy simulation modeling. *J. Fluid Mech.* 482:101–39

Sullivan PP, McWilliams JC. 2002. Turbulent flow over water waves in the presence of stratification. *Phys. Fluids* 14:1182–95

Sullivan PP, McWilliams JC, Melville WK. 2004. The oceanic boundary layer driven by wave breaking with stochastic variability. I: Direct numerical simulations. *J. Fluid Mech.* 507:143–74

Large-eddy simulation of an OBL with stochastic breakers and vortex force.

Sullivan PP, McWilliams JC, Melville WK. 2007. Surface gravity wave effects in the oceanic boundary layer: large-eddy simulation with vortex force and stochastic breakers. *J. Fluid Mech.* 593:405–52

Sullivan PP, McWilliams JC, Moeng CH. 2000. Simulation of turbulent flow over idealized water waves. *J. Fluid Mech.* 404:47–85

Teixeira MAC, Belcher SE. 2002. On the distortion of turbulence by a progressive surface wave. *J. Fluid Mech.* 458:229–67

Terray EA, Drennan WM, Donelan MA. 1999. The vertical structure of shear and dissipation in the ocean surface layer. *Proc. Symp. Wind-Driven Air-Sea Interface—Electromagn. Acoust. Sens., Wave Dyn., Turbul. Fluxes*. Sydney, Austr.: Univ. New South Wales

Terrill E, Melville WK, Stramski D. 2001. Bubble entrainment by breaking waves and their influence on optical scattering in the upper ocean. *J. Geophys. Res. Oceans* 106:16815–23

Thorpe SA. 2004. Langmuir circulation. *Annu. Rev. Fluid Mech.* 36:55–79

Thorpe SA. 2005. *The Turbulent Ocean*. Cambridge, UK: Cambridge Univ. Press

Thorpe SA, Osborn TR, Farmer DM, Jackson JFE, Hall AJ. 2003a. Measurements of turbulence in the upper ocean mixing layer using Autosub. *J. Phys. Oceanogr.* 33:122–45

Thorpe SA, Osborn TR, Farmer DM, Vagel S. 2003b. Bubble clouds and Langmuir circulation: observations and models. *J. Phys. Oceanogr.* 33:2013–31

Tsai WT, Hung LP. 2007. Three-dimensional modeling of small-scale processes in the upper boundary layer bounded by a dynamic ocean surface. *J. Geophys. Res.* 112:C02019

Tsai WT, Yue DKP. 1996. Computation of nonlinear free-surface flows. *Annu. Rev. Fluid Mech.* 28:249–78

Umlauf L, Burchard H. 2003. A generic length-scale equation for geophysical turbulence models. *J. Mar. Res.* 61:235–65

Measurements of separated flow over a water wave.

Veron F, Saxena G, Misra SK. 2007. Measurements of the viscous tangential stress in the airflow above wind waves. *Geophys. Res. Lett.* 34:L19603

Wanninkhof R, Asher WE, Ho DT, Sweeney CS, McGillis WR. 2009. Advances in quantifying air-sea gas exchange and environmental forcing. *Annu. Rev. Mar. Sci.* 1:213–44

Weller RA, Price JF. 1988. Langmuir circulations within the oceanic mixed layer. *Deep-Sea Res.* 35:711–47

Wright C, Walsh E, Vandemark D, Krabill W, Garcia A, et al. 2001. Hurricane directional wave spectrum spatial variation in the open ocean. *J. Phys. Oceanogr.* 31:2472–88

Zedler SE. 2007. *Strong wind forcing of the ocean*. PhD thesis, Univ. San Diego, Calif.

Zhou H. 1999. *Numerical simulation of Langmuir circulations in a wavy domain and its comparison with the Craik-Leibovich theory*. PhD thesis, Stanford Univ.

Annual Review of
Fluid Mechanics

Volume 42, 2010

Contents

Indexes

Errata

An online log of corrections to *Annual Review of Fluid Mechanics* articles may be found at http://fluid.annualreviews.org/errata.shtml